1

Fundamentals on Stress Changes

"We still do not know one thousandth of one percent of what nature has revealed to us"

— A. Einstein

1.1. Introduction

Earthquake generation is the result of the accumulation and release of strain on a given fault or fault segment. External stress produces deformation (strain), which under elastic conditions leads eventually to failure. The elastic deformation is instantaneous and is completely recoverable when the applied stress is removed. When a linear relation exists between the applied stress and the resultant strain, the material is characterized as purely elastic. This assumption is a good approximation for small deformations. In the case where the material continues to deform beyond the elastic limit, it undergoes permanent deformation and failure occurs due to the breakdown of interatomic bonds.

Earthquakes are generated by displacement on discontinuities in the elastic part of the lithosphere, with the seismogenic faults assumed to maintain the elastic properties. The continuous plate motion loads the faults and

fault segments that are located along the plate boundaries, for example, and the resulting accumulated strain will culminate in a slip onto the fault surfaces. Given that the plate motion is considered stable, the strain loading and release is expected to be regular in time, unless these fault segments are not expected to follow the stick and slip stages completely independently. Successive earthquake occurrences are usually interdependent [SCH 90]. This implies that a slip on one segment seems to "load" or "unload" adjacent segments, and thus their earthquake recurrence cannot be independent. This suits the observation that their reoccurrence does not take place in regular interseismic periods. Accumulation of strain, which governs the earthquake recurrence times, differs among different areas since the strain rate depends on the tectonic activity as the relative plate motion. At the interface between adjacent plates, for example, the strain rate acquires its maximum values, which resulted in the most frequent and largest earthquakes. In continental regions where the rates of strain accumulation are lower, whereas the seismicity is more diffused, appropriate approximations are required to achieve estimates of the anticipated earthquake hazard.

Despite substantial advances in our understanding in the last decades since the associated faults are interacting through their stress field, we still have a long way to go to achieve reliable estimates of the recurrence times of stronger earthquakes associated with the major faults in a given area. This highlights the requisiteness for intensifying our efforts towards identification of the location and occurrence time of the anticipated strong earthquakes. Substantial progress has been made in identifying the source regions of future earthquakes by stress interaction modeling, which led to the assessment that the slip during the occurrence of a strong earthquake changes the stress field and increases the likelihood for the occurrence of nearby earthquakes. Outstanding examples are the stress calculation after the

preferential occurrence of the aftershocks of the 1992 Landers main shock ($M_w = 7.3$) [KIN 94] and the along-strike sequential occurrence of large earthquakes in the North Anatolian Fault [STE 97], which will be presented in more detail in the following sections. Although these cases, along with a considerable number of earthquake occurrences, were consistent with these forecasts, other earthquake forecasts based on the relevant approach were not verified. The recognition that stress changes considerably influence the time and place of the next earthquake has been reviewed in [HAI 10].

The earthquake-prone areas encompass fault zones containing a large number of faults, with the location of some of them being unknown, and for this reason, several recent devastating earthquakes are associated with faults whose hazard was inadequately assessed. The Coulomb stress changes caused by the displacement in the occurrence of strong earthquakes associated with specific faults and fault segments in a fault population were confirmed to be ample to explain many seismic observations, including aftershock locations, spatial evolution of earthquake series and absence of expected shocks in active regions after the occurrence of strong earthquakes. This is due to the fact that the failure of one fault segment transfers stresses to the nearby segments, which encourages or discourages more earthquakes associated with these faults. Therefore, fault interaction is an indispensable component for any seismic hazard assessment. The effect of the Coulomb stress changes has a remarkable impact on the distances of two or three fault lengths. Remote triggering at distances equal to several fault lengths, which can reach thousands of kilometers, depending on the magnitude of the causative earthquake, has been observed; however, after a strong earthquake, it is perfectly determined by the propagation of transient (dynamic) seismic waves because they are capable of inducing failure either immediately or by delayed triggering. The triggering role of

the passage of seismic waves is mainly important in the near field.

The assessment of the earthquake forecasts based on the calculation of stress changes is mainly performed with the available earthquake catalogs that span a duration (100–150 years) much shorter than the recurrence intervals of the strong earthquakes in a given study area, which may take values of hundreds to thousands of years. This is the main reason why many strong earthquakes cannot be forecasted, thereby making a deterministic seismic hazard assessment more uncertain. Stress modeling has proved to be effective in most of the places where it is applied; nevertheless, it is not adequate for an integrated seismic hazard assessment because it has been accomplished in mapped (already-known) active faults. For this purpose, we need to use techniques that can reveal the anticipated hazard by modeling complex interactions using mathematical analysis together with stress changes calculations, based on and interpreted with realistic physical models.

1.2. Stress interaction

The occurrence of an earthquake is influenced by the slow continuous tectonic loading along with the stress changes due to the coseismic slip of the previous earthquakes; in particular, the stronger and the closer ones that occur close together both in time and space (otherwise a time “delay” is observed in the occurrence of an anticipated earthquake) manifest these stress interactions, meaning that during an earthquake occurrence, the stress transferred to the neighboring faults may increase or decrease the stress onto them, and in this way, it may enhance or inhibit earthquake occurrence there. Earthquake interaction is of particular interest to understand whether strong earthquakes cluster both spatially and temporally, occurring in time intervals of some months or years, or even in shorter time frames, instead

of hundreds of years, which is the typical recurrence time of such earthquakes when the associated faults are considered individually.

The state of stress is examined soon after an earthquake occurs, considering that the stress is released from the activated fault. The causative fault remains inactive during the interevent time, which represents the time for this certain fault reactivation, i.e. the time that the stress needs to be rebuilt and released again in the second earthquake, typically hundreds to thousands of years. When an earthquake occurs, the stress is not dissipated, with its changes exhibiting a certain spatial pattern around the fault that failed, and particularly at the fault tips. These stress changes were found to be related to changes in seismicity behavior and triggering at distances much longer than the fault length and for stress changes as small as 0.1 bar [REA 92, KIN 94]. In any case, an earthquake occurs by stress which triggers only when the fault is in the late phase of its seismic cycle, meaning that it is already mature and close to failure. The stress state of the particular fault or fault segment might be evaluated on the basis of its known stressing rate and recurrence history.

Therefore, the recurrence time of strong earthquakes depends on the long-term tectonic loading, which is assumed constant with time, the stress drop during the earthquake occurrence and the stress at which the fault failed (failure stress). Stress changes may modify the mean return period and cause either advancement or retardation of the next earthquake occurrence. This time shift (Δt, in years) is simply expressed as $\Delta CFS/\tau$, where ΔCFS is the Coulomb stress change (Coulomb failure stress) mainly attributed to the coseismic static stress changes and τ is the continuous tectonic loading. This impact on the occurrence time is called either “clock advance” (in the case of stress loading) and “clock delay” (in the case of stress relaxation) for the cases of

stress enhancement and stress inhibition, respectively. For example, the subsequent strong earthquakes on the fault segments of the San Andreas Fault are found, which occurred almost a decade ago in the anticipated time of occurrence of great earthquakes, by the 1992 Landers sequence of earthquakes [JAU 92]. Simpson *et al.* [SIM 88] found that the 1983 Coalinga earthquake inhibited the occurrence of the subsequent moderate Parkfield shock for about one year.

The changes in the stress field are the result of strain accumulation and release in the brittle layer according to the seismic cycle concept. This is based on the assumption that the static stress changes caused by an earthquake occurrence are completely recovered during the interseismic period, meaning that the total of stress equals zero. This also perfectly agrees with the time-predictable model. The assumption is that the static stress change at the time of occurrence of a strong earthquake is completely recovered during the period of strain accumulation, i.e. the net change in stress over the earthquake cycle is zero. This assumption is equivalent to the time-predictable model of earthquake occurrence [SHI 80]. Stress changes are either "static", resulting from the coseismic slip and taking place instantaneously and permanently, or "dynamic", caused by the passage of seismic waves, in which case they are oscillatory and transient. Dynamic and static stress changes cannot be distinguished either observationally or theoretically at short times and distances from an earthquake, and both approximately attenuate as some inverse power of the distance is caused when the seismic waves travel through and are oscillatory and impermanent. In the near field and soon after the occurrence of a strong earthquake, the impact of either the static or dynamic stress changes cannot be discriminated, whereas both rapidly decrease in value when the distance from the fault increases [STE 05]. In longer distances, the static stress changes attenuate faster, approximately following the inverse of the

cube of the distance from the source, while the dynamic stress changes arrive at longer distances in a distinctly different way since their attenuation rate is lower. Coseismic Coulomb stress changes and their interrelation with the aftershock epicentral distribution were initially investigated in [DAS 81]. Nevertheless, it has become popular since the occurrence of the 1992 Landers ($M = 7.3$) earthquake [STE 92]. The estimated values of the stress changes that are often found to have promoted the occurrence of large earthquakes on neighboring faults or fault segments are approximately equal to a small percentage of the stress drop on the ruptured fault, being generally in the range of 20–30 MPa. The values of the stress related to triggering are a hundred to a thousand times lower. Given that the stress drops and the triggering times, either advances or delays, are smaller than the earthquake recurrence times, the evidence is provided that both faults, the causative fault and the target fault, are required to be synchronized and at the ultimate state of their seismic cycles. Paleoseismological data show that for the same regions, prior earthquakes have occurred in clusters of ruptures of several faults separated by long quiescent periods [SCH 10]. Theoretical and experimental data reveal that synchronization may happen at the positive stress coupling area between adjacent fault segments and slip rates ranging in between certain conjugation thresholds.

Among the globally known cases of earthquake interaction are the $M \geq 7.0$ triplet that took place in: (a) 1811–1812 in New Madrid (USA) [WIL 10]; (b) the sequential along-strike occurrence in the Anatolian Fault (NAF) that started in 1939 [STE 97], which culminating with two earthquakes with $M \geq 7.0$ that occurred in less than two months temporal distance along two adjacent fault segments in 1999 [PAP 01a]; and (c) the two $M > 8.5$ Sumatra earthquakes that occurred within a few months in 2004 and 2005 [MCC 05]. The notable example of the NAF in 1999 is depicted with the spatial variations of the calculated

Coulomb failure function (ΔCFF) expressing the changes caused by the coseismic slip of the $M_w = 7.4$ earthquake of August 17, 1999 that struck a segment in NW Turkey in the area of Izmit Bay (Figure 1.1). The stress pattern shown in Figure 1.1 was calculated in accordance with the fault plane solution of the main shock, i.e. a vertical strike-slip faulting [PAP 01b]. Large positive values of ΔCFF are well correlated with the distribution of strong aftershock foci and also with the adjacent eastern fault segment, where the 1766 event of $M = 7.3$ was generated, implying possible triggering of this segment, which effectively failed in a relatively short time on November 12, 1999 with the $M = 7.2$ Düzce main shock.

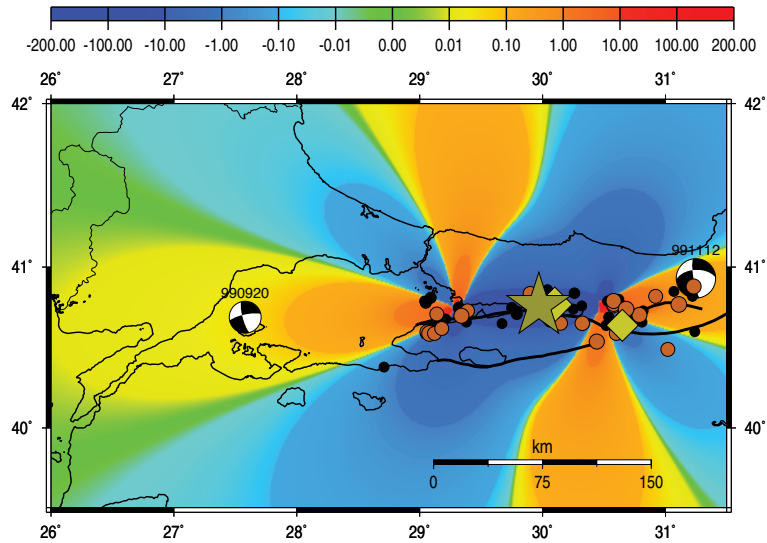

Figure 1.1. *Coseismic Coulomb stress changes (ΔCFF) caused by the August 17, 1999 Izmit main shock of North Anatolian Fault, resolved in agreement with the min shock faulting type (vertical right-lateral strike-slip fault). The locations of the $M \geq 4.4$ aftershocks, taking place during August 17–September 30, 1999, are superimposed. The focal mechanism of the triggered Düzce main shock (November 12, 2001, $M_w = 7.0$) is depicted as an equal-area lower-hemisphere projection and plotted at the epicenter, where the positive Coulomb stress changes have taken values of about 1 bar (source: [PAP 01b]). For a color version of this figure, see www.iste.co.uk/votsi/multistate.zip*

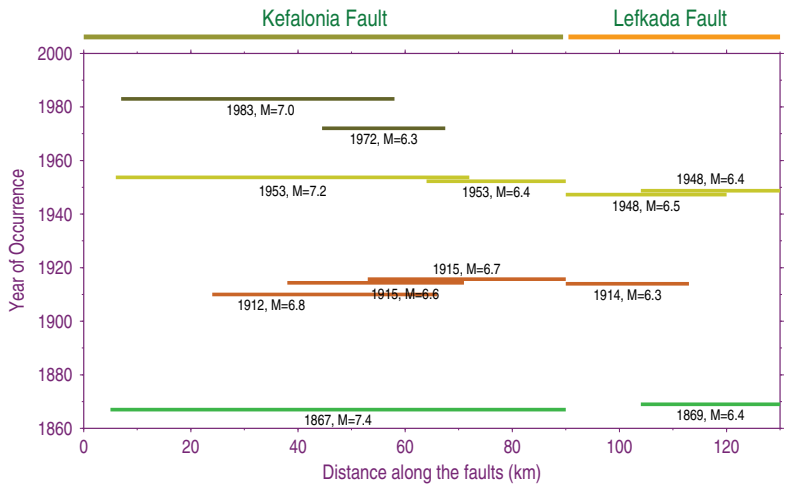

Figure 1.2. *Temporal presentation of the activated major faults in the Kefalonia Transform Fault Zone (KTFZ) along the Kefalonia branch, whose strike is* $\sim N50^oE$*, and the Lefkada branch, whose strike is* $\sim N10^oE$*, since 1867. The solid lines indicate the corresponding rupture lengths. Modified from [PAP 02]. For a color version of this figure, see www.iste.co.uk/votsi/multistate.zip*

Synchronization of two adjacent fault branches was identified along the Kefalonia Transform Fault Zone (KTFZ). From the spatiotemporal distribution of strong ($M \geq 6.3$) crustal earthquakes originated on one of the two branches, namely on the Kefalonia or Lefkada branch of the KTFZ, it resulted that they were clustered in relatively short time intervals (of the order of a few years) alternating with much longer, relatively quiescent periods [PAP 02]. In each active period, there was a relatively large event or a series (two to four) of events, close in time and abutting or slightly overlapping with rupture zones (Figure 1.2). This synchronization has been estimated to take place four times since 1867, i.e. since when the available earthquake catalog [PAP 97] was verified for its completeness at this magnitude threshold. This seismic behavior was investigated through the calculations of Coulomb stress changes caused by the coseismic displacement of the consecutive events and the

continuous slow tectonic loading on the activated fault segments. The result was that in 13 out of 14 cases, the forthcoming earthquakes were in stress-enhanced area values, i.e. from 0.01 MPa to higher than 0.1 MPa. This implies that the observed synchronization is well supported by stress transfer among neighboring fault segments in a fault population.

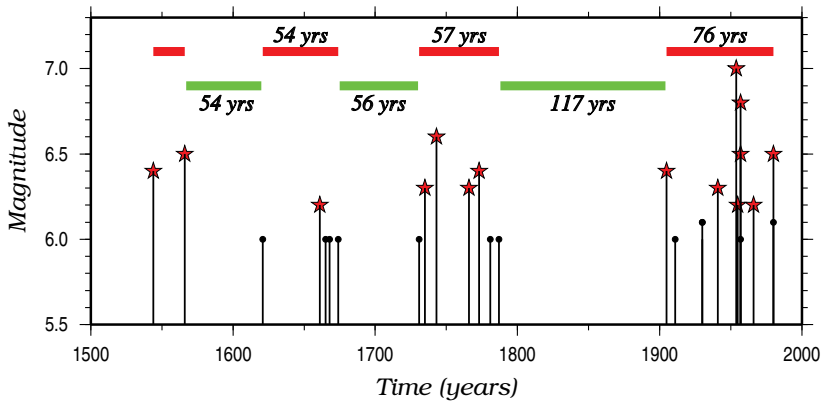

Figure 1.3. *Temporal distribution of earthquake magnitudes, where clustering and quiescence periods are shown. The alteration of active and inactive periods and their durations are indicated by bars and are given in years on the top of the figure. Modified from [PAP 03]. For a color version of this figure, see www.iste.co.uk/votsi/multistate.zip*

One more remarkable example from Greece concerns the episodic occurrence of $M \geq 6.2$ earthquakes in the Thessalia Fault Zone between 1954 and 1957, when three seismic sequences took place and where no such events had occurred in about two centuries [PAP 03]. Figure 1.3 shows a magnitude–time plot, where the aforementioned behavior is illustrated from 1500, i.e. from when the earthquake catalog [PAP 97] was considered complete. The stars denote earthquakes with $M \geq 6.2$, whereas the circles denote the $6.0 < M < 6.2$ ones; this distinction has been made to secure a

reliable magnitude estimation. Four active periods are found to be alternating with inactive ones. As far as the 20th Century is concerned, it resulted that all events were generated in areas of positive stress changes because of the displacements during the occurrence of previous shocks and the continuous tectonic loading on the active faults in the area.

Fault interaction encompasses dynamic stress changes, in addition to the static ones, which are time-varying and transient. Although static stress changes are critical for aftershocks close to the rupture, in distances longer than one fault length, they are even smaller than tidal stresses. The changes in dynamic stress are caused by the seismic waves that transmit transient oscillatory stresses that do not permanently alter the net load of the fault, but its mechanical state. Dynamic stress changes were capable of explaining remote triggering as well as the aftershock activity. For the $M_w = 7.3$ 1992 Landers earthquake, Kilb *et al.* [KIL 00] found similar asymmetries in the aftershock pattern and the dynamic stress pattern. Following the 1999 $M_w = 7.4$ Izmit (Turkey) main shock, an intensification of seismicity in the Greek territory took place, at distances of 400–1000 km from the main rupture [BRO 00]. Small events occured soon after the surface waves of the main shock passed through the probably triggered area. In contrast to the case of the Landers main shock with long-distance triggering, the activated areas are clearly non-volcanic. It has been found that dynamic triggering of seismicity takes place in geothermal and magmatic fields [HIL 93]. A spatial correlation between geothermal and activated areas is feasible, although the recent magmatism does not exist in the study area.

The strength of the triggering waves can be measured either by the amplitude of the transient stress, which scales as the particle velocity, or by the energy density delivered by

the waves. A physical mechanism is required to transform the transient stresses of the seismic waves into sustained stresses on the fault capable of producing an earthquake, hours or days later, and several possible mechanisms have been suggested (see, for example, [HIL 93, GOM 98]). The most favorable interpretation is based on fluid mechanics, because both observed triggering and geothermal activity take place in tectonic environments where stretching is the dominant style of active deformation.

1.3. Stress changes calculation

The modeling of static stress changes can be calculated easily enough, whereas the absolute values of the stress cannot be measured. The modeling requires knowing the fault geometry and the sense and magnitude of the coseismic slip, the details of which, in turn, become less significant when the distance of the observation point from the rupture increases [AKI 02]. Stress changes associated with coseismic displacements are calculated using a disclocation model of a planar fault surface Σ, which is assumed to be embedded in a homogeneous elastic half-space, for the displacement calculations. According to Steketee [STE 58], the displacement field component, u_k (k^{th} component of u), in the aforementioned model and for an arbitrary uniform dislocation U, onto Σ, is calculated as

$$u_k = \frac{U_i}{8\pi\mu} \int \int_{\Sigma} w_{ij}^k v_j d\Sigma, \qquad [1.1]$$

where μ is the shear modulus, v_j are the direction cosines of the normal to the dislocation surface, U_i is the i^{th} component of U and w_{ij}^k are six sets of Green's functions. The displacements and strain components are calculated by the integration [1.1] [OKA 92]. The elastic stress tensor components, s_{ij}, are estimated according to Hooke's law,

assuming an isotropic medium from the elastic strain components, e_{ij},

$$s_{ij} = \frac{2\mu\nu}{1-2\nu}\delta_{ij}e_{kk} + 2\mu e_{ij}, \qquad [1.2]$$

where ν is Poisson's ratio and δ_{ij} is the Kronecker delta.

The faults fail when the stress onto them overpasses their strength. The failure proximity was measured by the Coulomb failure function changes (ΔCFF) (given by [SCH 90, HAR 98] and the references therein).

These changes caused by the displacement during the main shock occurrence are estimated by the following equation:

$$\Delta CFF = \Delta\tau + \mu(\Delta\sigma + \Delta p),$$

where $\Delta\tau$ and $\Delta\sigma$ are the changes in the shear and normal stresses, respectively, onto the fault plane, and Δp is the change in pore pressure in the rupture area. Both $\Delta\tau$ and $\Delta\sigma$ are estimated from the stress tensor given in [1.2] for the causative fault plane. Change in shear stress $\Delta\tau$ is considered positive when shear stress increases in the direction of slip; $\Delta\sigma$ is positive when the tensional normal stress increases. When the compressional normal stress decreases, the static friction onto the fault plane also decreases. When both $\Delta\tau$ and $\Delta\sigma$ are positive, the fault approaches failure; negative $\Delta\tau$ and $\Delta\sigma$ move the fault away from failure. A positive value of ΔCFF indicates that the fault is approaching failure. This may happen when the shear stress is increased or when the effective normal stress, $\mu(\Delta\sigma + \Delta p)$, is decreased. The pore pressure change during the coseismic phase, when the porous medium is considered to still be in undrained conditions [RIC 76], is given by

$$\Delta p = -B\frac{\Delta\sigma_{kk}}{3},$$

where B is Skempton's coefficient ($0 \leq B < 1$), which depends on the bulk moduli of the medium and the volume percentage completed by fluid, and $\Delta\sigma_{kk}$ is the trace of the induced stress tensor. Rock experiments suggest typical values of B ranging between 0.5 and 0.9 [ROE 96].

An alternative interpretation is based on the fact that the material of the fault zone is more ductile than the material in the surrounding area, which results in equality of the normal stress components, $\sigma_{xx} = \sigma_{yy} = \sigma_{zz}$, and in this case, $\Delta\sigma_{kk}/3 = \Delta\sigma$ in the fault zone. Under these conditions, i.e. a homogeneous and isotropic medium outside and homogeneous and isotropic inside the more ductile fault zone, it is derived that

$$\Delta CFF = \Delta\tau + \mu'\Delta\sigma.$$

Here, μ is the apparent friction coefficient, ranging between 0.6 and 0.8 (see [HAR 98] and the references therein) and $\mu' = \mu(1 - B)$. The parameter μ' is the apparent friction coefficient for including the influence of pore fluids along with the material properties of the fault zone. For the homogeneous isotropic poroelastic model, μ' is the function of $\Delta\sigma_{kk}$ and $\Delta\sigma$:

$$\mu' = \mu\Big(1 - \frac{\beta'}{3}\frac{\Delta\sigma_{kk}}{\Delta\sigma}\Big).$$

The parameter β' for rock is contiguous to Skempton's coefficient B for soils and depends on the bulk moduli of the material and the percentage of the fluid filling in the material. The undrained case is usually considered [BEE 00], where Δp depends on the normal stress change on the observational fault plane. The selection of an appropriate value for μ is demanded for the modeling. The μ' value in coseismic static stress changes calculations is determined to be between 0.0 and 0.75. The most widely accepted value, i.e. 0.4, was suggested by [KIN 94], who found that

fluctuations of the friction coefficient resulted in a subtle influence on aftershock correlations.

The variation of friction coefficient values influences the values of Coulomb stress changes and, to a lesser extent, their spatial pattern. Smaller friction coefficient values result in smaller Coulomb stress changes, since the resistance to coseismic slip is smaller. Thus, the coseismic stress drop is lower, also leading to smaller Coulomb stress changes on the receiver faults.

1.4. Modeling of Coulomb stress changes for different faulting types

Stress is a tensorial quantity that changes in space and time. Similarly, the stress field spatial representation considerably changes on most target faults when faulting geometry and kinematic properties are varied. Thus, the sign of the Coulomb stress changes (ΔCS) should be investigated as a function of certain faulting type. At a given site, a stress-enhanced area for an E-W striking normal fault and a stress-inhibited area for any other faulting representation can be observed. The dip of the target fault considerably affects the static stress changes. Variations in dip angle modify the spatial variations of positive and negative stress changes. In this way, a fault plane located inside a stress-enhanced area could be placed in a stress-inhibited area.

1.4.1. ΔCS *for strike-slip faulting*

Calculations of Coulomb stress changes were first performed for several cases of vertical strike-slip faults, given that this faulting geometry facilitated the presentation and interpretation of the spatial distribution of these stress changes. In order to investigate the influence of the 1992

Landers $M = 7.4$ main shock on the future hazard of the San Andreas Fault system, King *et al.* [KIN 94] examined the possible triggering of one earthquake by another. It was found that the distribution of aftershocks along with several other moderate nearby earthquakes might be determined by the Coulomb criterion in that aftershocks are abundant, where the Coulomb stress was larger than 0.5 bar, and sporadic seismicity in places with Coulomb stress decreases by the same value. It has been found that the 1992 $M = 7.4$ strike-slip Landers earthquake triggered the $M = 6.5$ strike-slip Big Bear earthquake associated with a neighboring fault segment by increased static stress changes values equal to 0.3 MPa. The spatial pattern of the stress field inverted according to an almost vertical strike-slip receiver fault is shown in Figure 1.1.

1.4.2. ΔCS *for dip-slip faulting*

Studies on static stress changes on dip-slip faults follow, and the first attempts concern the 1980 Irpinia (Italy) normal fault earthquake. The results were analogous to those in the strike-slip cases, revealing stress enhancement on the neighboring strike-slip Potenza fault, which activated in 1990 and 1991 [NOS 97]. In the same way, an earthquake series that took place at the South Lunggar Rift (Tibet) between 2004 and 2008 is perfectly explained by stress transfer among the failed fault segments [RYD 12]. The first 2004 main shock put an along-strike receiver fault in positive stress changes, which failed in 2005. This latter increased the positive static stress changes onto two antithetic faults that ruptured in 2008. [RYD 12]. In the back arc Aegean region, dominated by N-S extension, relative clustering in strong earthquake occurrence alternating with relatively quiescent periods was satisfactorily interpreted by stress transfer among the fault segments comprising in a fault population, like that in the southern Aegean [PAP 05] and Northern Greece and Bulgaria [PAP 07]. An example is given here of the stress

field changes calculation and the resultant triggering, from the cascade occurrence of four $M \geq 6.0$ seismicities in the Thessalia district (Greece) between 1954 and 1957, along with the activation of two contiguous faults in 1985. Figure 1.4 depicts a regional map with the focal mechanisms of these earthquakes plotted at the location of their epicenter, whereas the year of occurrence is designated above the beach ball that represents their fault plane solution. From the position of the inferred surface traces of the faults associated with each earthquake, it is evident that they comprise a fault population, namely adjacent fault segments that fail with the same mechanism. It is worth noting that the two doublets of 1957 and 1980 had a few minutes' time difference in their occurrence. Although Coulomb stress changes can explain possible triggering (prompt, like in the doublets of 1957 and 1980, or delayed, like the other events), it is not feasible to assess sequential occurrence.

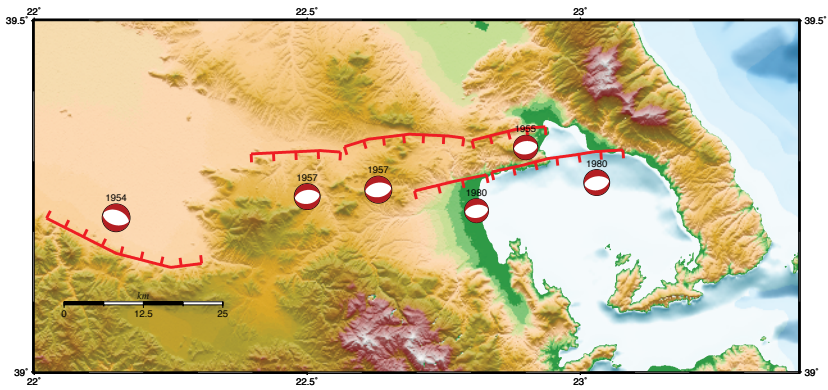

Figure 1.4. *Focal mechanisms of the $M \geq 6.3$ shocks associated with faults bounding along the southern basin periphery shown as equal-area lower-hemisphere projections with their year of occurrence written above and mapped at their epicentral position. The inferred surface expression of the causative faults are also plotted, with the ticks showing their dipping direction. For a color version of this figure, see www.iste.co.uk/votsi/multistate.zip*

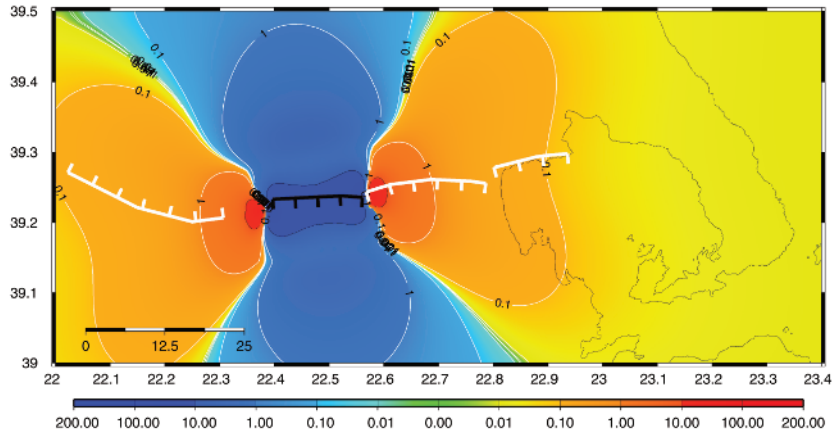

Figure 1.5. *Coulomb stress changes associated with the occurrence of the 1957/03/08 $M6.5$ earthquake in the southern margin of Thessalia basin, central Greece, inverted according to the faulting type of the source fault at 8.0 km depth and static stress changes (in bars) given according to the color scale. The fault surface expressions are depicted by white lines, with the ticks showing the dip direction, whereas the causative fault is shown in black. For a color version of this figure, see www.iste.co.uk/votsi/multistate.zip*

Figure 1.5 presents the spatial pattern of the static stress changes that are due to the coseismic displacement of the 1957/03/08 earthquake with $M = 6.5$ and the evaluation of their impact in the adjacent fault segments. These changes are computed in agreement with the sense of slip on the fault that failed 80/40/–90 and at a depth of 8 km. The major faults of this faulting network are plotted at their inferred surface fault traces. The red areas represent stress increase, the blue represents stress decrease and the black and white represent causative and adjacent major regional faults, respectively. From a visual inspection, all neighboring faults are located inside stress-enhanced areas. The positive static stress changes are comprised in lobes beyond the fault edges, revealing increased stress concentration. The next earthquake occurred just after seven minutes, on the eastern

adjacent fault segment. It should be mentioned at this point that an earthquake of $M = 7.0$ occurred in 1954 on this fault, which was the first and the strongest in this seismic excitation. It is worth noting that the along-strike adjacent normal faults are inside the positive lobes where the Coulomb stress changes obtained their maximum values.

Similar fault interactions after major earthquakes were inferred for contractional tectonic settings. For example, Lin *et al.* [LIN 11] linked the majority of the aftershocks of the 2003 $M_w = 6.9$ thrust fault Zemmouri (Algeria) earthquake to an increase in coseismic Coulomb stress change. The analysis of static Coulomb stress changes after the 2008 $M_w = 7.9$ Wenchuan earthquake, which ruptured the Beichuan and Pengguan reverse faults, showed significant static stress changes, either positive or negative, on the regional faults. Static stress interactions were also sought for thrust faulting environment. Lin *et al.* [LIN 11] associated most of the aftershocks of the 2003 $M_w = 6.9$ thrust fault Zemmouri (Algeria) earthquake with positive coseismic Coulomb stress change. The coseismic slip of the 2008 $M_w = 7.9$ Wenchuan earthquake associated with the Beichuan and Pengguan reverse faults, resulted in significant static stress changes, either positive or negative, on the regional faults [PAR 08]. Figure 1.6 shows the Coulomb stress changes associated with the coseismic slip of an $M_w = 6.7$ main shock in 2013 that occurred on a certain fault segment along the western Hellenic arc. Although the spatial pattern is quite similar to the one shown in Figure 1.5, containing four main lobes for positive and negative values of the ΔCS, the considerably shallower fault dip resulted in less symmetry in their shape.

The location of the dip-slip faults in relation to the causative fault, either normal or thrust ones, also influences the received static stress changes. The displacement fields for normal and thrust faulting are considerably different.

Nevertheless, failure for both types of this dip-slip faulting type is discouraged if the receiver faults are directly located in the hanging wall and footwall of the causative fault. This happens because the coseismic displacements in the upper crust counteract the sense of slip on the receiver faults. Regardless of the faulting type, either stretching or contraction, the maximum positive stress changes are located around the fault tips as well as in smaller areas onto the hanging wall of the target faults and the footwalls of the causative faults. The Coulomb stress changes were calculated assuming a slip model without heterogeneities that emerge from the particular earthquake generation mechanism, localized strength and frictional variations.

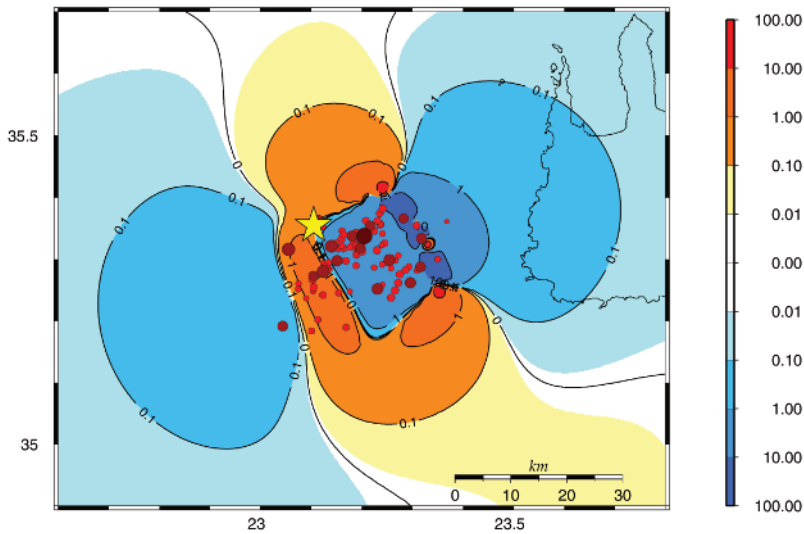

Figure 1.6. *Coulomb stress changes due to the 2013 ($M_w = 6.7$) earthquake coseismic slip that occurred in the western Hellenic arc, resolved for a thrust faulting type. The epicenters of the main shock and its aftershocks are shown by the asterisk and circles, respectively, with aftershock epicenters colored and sized according to the corresponding event magnitude. For a color version of this figure, see www.iste.co.uk/votsi/multistate.zip*

1.5. Seismicity triggered by stress transfer

Fault interaction was investigated in several cases on a regional scale by evaluating stress spatial distribution for diverse faulting types according to the characteristics of the regional fault network. Static stress changes transferred from the causative to the neighboring receiver faults and, in several cases, the accumulated stress changes that included the long-term tectonic loading were revealed. Stress triggering takes place because of the stress redistribution caused by the coseismic slip in the main rupture. During an earthquake, the built-up elastic stress in the crust is relieved, and at the same time, the stress in certain regions is unambiguously increased by the coseismic slip. The faults comprised in these regions are mature enough, meaning at the late stage of their seismic cycle, to be possible candidates for failure by triggering. This may occur very fast, like the Big Bear earthquake that occurred only hours after the Landers earthquake; after several years, like the Hector Mine earthquake that occurred seven years after the Landers earthquake; or after several decades, like the 1995 $M = 6.9$ Kobe (Japan) main shock that is considered to be triggered by the 1944 $M = 8.0$ Tonankai and the 1946 $M = 8.2$ Nankaido earthquakes [POL 97].

1.5.1. *Triggering of strong earthquakes*

The significance of earthquake interaction investigation points to the feasibility of predicting the sites of the future earthquakes. In the cases where the triggering of strong earthquakes is sought, the stress changes are estimated after considering the coseismic slips on the important fault segments in a fault population and summing the changes of each stress tensor component as they occur in time [DEN 97a]. These authors computed the Coulomb stress changes caused by the coseismic slips of seven $M \geq 7.0$ main

shocks that have occurred since 1812 along with the tectonic loading on the major regional faults in southern California. It was found that 95% of the $M \geq 6.0$ earthquakes generated by either strike-slip or reverse faulting occurred in stress-enhanced areas. After continuing this investigation in [DEN 97b], it was confirmed that more than 85% of the $M \geq 5.0$ earthquakes that occurred between 1932 and 1995 were located in areas of positive static stress changes, whereas the remaining 15% are located adequately close to the borders between positive and negative stress change areas. In North Aegean and northwest Turkey, it was found that since 1912 four times more earthquakes are correlated with increased Coulomb stress due to the coseismic slips of previous events in the dataset [NAL 98]. Papadimitriou and Sykes [PAP 01b] investigated the evolving stress field in the 20th Century in North Aegean by considering, in addition to the strong main shocks, coseismic slip along with the slow tectonic loading on the significant fault segments in the study area, and calculating the stress changes according to the focal mechanism of the next earthquake whose triggering was inspected. The calculations revealed that large earthquakes occurred in stress-enhanced areas, whereas most of the moderate shocks with known focal mechanism were also located in areas of positive ΔCFF.

A notable case concerns the sequence of earthquakes in the area of western Sichuan, where frequent strong ($M \geq 6.5$) earthquakes occurred, with most of them associated with fault segments belonging to the sinistral strike-slip Xianshuihe fault zone, with a total length of 350 km. From both historical information and instrumental recordings, the alteration of highly active periods with quiescent ones was verified, along with a notable epicentral migration. In the most recent active period, the rupture areas of strong earthquakes were abutting and covered the entire Xianshuihe fault. Papadimitriou and her colleagues [PAP 04]

investigated the possible triggering of each earthquake by the previous ones by calculating the evolution of the stress field since 1893. The changes in the static stress changes were calculated after considering the coseismic slip of the strong ($M \geq 6.5$) earthquakes and the long-term slip rate on the different fault segments and inverted according to the faulting type of the faults of interest.

The calculations showed that all of the strong events and most of the moderate-magnitude ones, with a known focal mechanism, were in areas of increased Coulomb stress. This adds more value to the calculation technique of Coulomb stress, which is a powerful tool for forecasting future seismic activity (Figure 1.7). By extending the stress changes calculations up to 2025, the seismic hazard was estimated to be ensuing for the fault segments that are found in stress-enhanced areas.

1.5.2. *Aftershock triggering*

The positive Coulomb stress changes are not only located at the tips of the causative faults, but they also form off-fault lobes where the aftershock activity is expected to be triggered. The interpretation of aftershock occurrence beyond the fault tips was first given by [DAS 81], who indicated that the aftershocks have occurred in specific locations where crack models predict an increase in stress resulting from the main shock rupture. Large stress increases were noted near the crack tip, but in addition, there were small stress increases on either sides of the crack or about one crack away. These were the regions in which off-fault aftershocks were often seen alike in the case of the $M_w = 6.4$ July 26, 2001 Skyros (North Aegean, Greece) main shock that occurred in the western part of the North Aegean Sea [KAR 03].

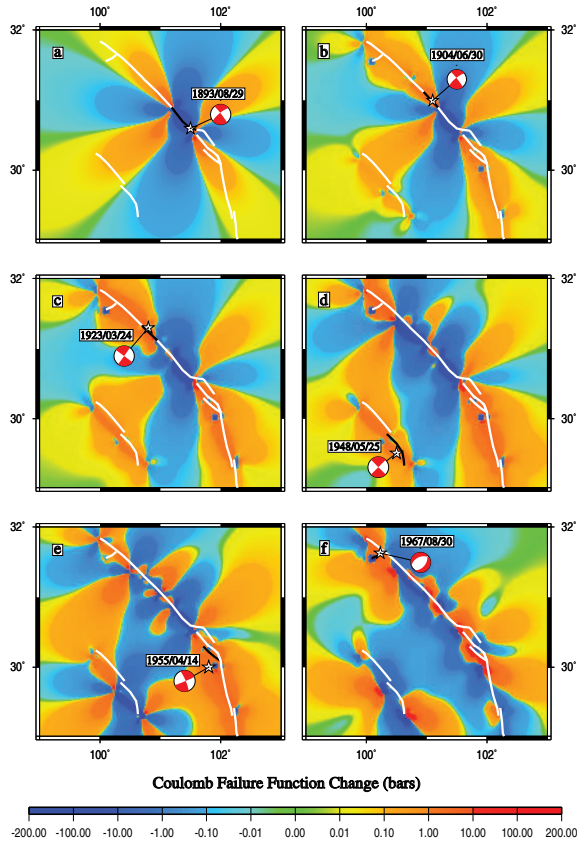

Figure 1.7. *Stress evolution along the Xhianshuihe and Litang fault zones since 1893, calculated at a depth of 8.0 km. The stress changes are calculated each time for the faulting type of the next strong event and are denoted by the color scale at the bottom (in bars). Fault plane solutions are plotted as lower-hemisphere equal-area projections, on the top of which the occurrence date (year/month/day) is written. The fault traces are depicted by white lines, and the fault segment associated with the occurrence of each event in each stage of the evolutionary model is shown in black. (a) Coseismic Coulomb stress changes associated with the 1893 event. (b) Stress evolution until just before the 1904 event. (c) ΔCFF just before the 1923 event. (d) Stress evolution until just before the occurrence of the 1948 event. (e) State of stress just before the 1955 event. (f) Stress evolution just before the occurrence of 1967 event, calculated for normal faulting type (modified from [PAP 04]). For a color version of this figure, see www.iste.co.uk/votsi/multistate.zip*

The seismicity forms three distinctive clusters aligned in different directions, which also differ from the known normal and right lateral strike-slip faults in the study area. The Coulomb stress changes that are caused by the main rupture were calculated, and the stress-enhanced areas are consistent with the off-fault aftershock activity (Figure 1.8), showing a means for the evaluation of the seismic hazard emerging for the strong aftershocks that occur far from the main shock epicenter. For securing the robustness of this result, the ΔCS values were calculated for a range of frictional parameters and fault geometry (Figure 1.8) and the findings were further supported.

On August 14, 2003 a strong ($M_w = 6.2$) main shock took place in the Lefkada Island (Central Ionian). Numerous aftershocks occurred at distances of more than 40 km beyond the fault tip, with a dense cluster, in particular, well located inside a lobe where the positive ΔCS values became higher (Figure 1.9). Theoretical static stress changes from the main shock provide a plausible interpretation for the off-fault aftershock activity and the triggered seismicity associated with the adjacent fault and further evidence for seismic hazard associated with this fault [KAR 04].

The static stress changes due to the coseismic slip of the 1995 $Mw = 6.5$ Kozani-Grevena (Greece) main shock on the aftershock locations of 173 aftershocks recorded between six and 12 days after the main shock were investigated in [LAS 09]. A detailed rupture model (comprising three sub-faults), relocated aftershock epicenters and reliable fault plane solutions are used for this scope. A statistical testing method was developed, which investigated the possibility that the same set of aftershocks inside a certain area, whose occurrence was attributed to the given static stress changes, would be there even without any influence in the stress changes due to the coseismic slip of the main shock. These changes were computed at each aftershock focus and for both nodal planes (Figure 1.10).

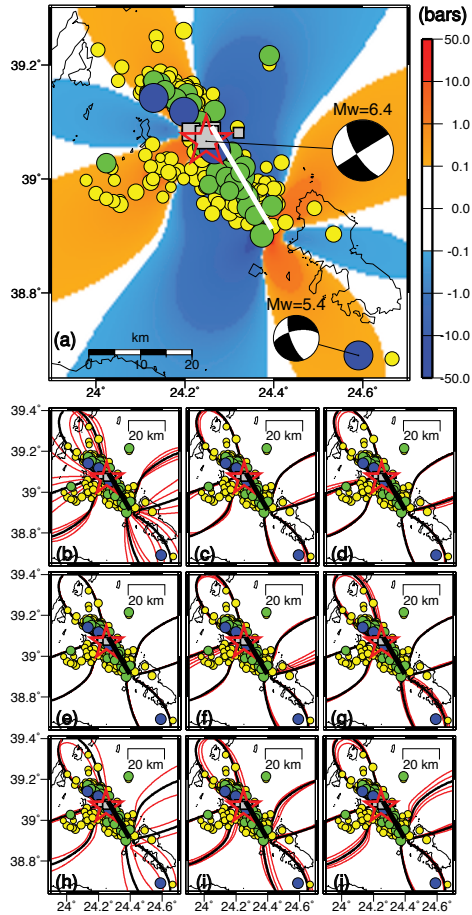

Figure 1.8. *(a) Coulomb stress changes (in bars), caused by the 2001 Skyros main shock, for a target plane with strike* $= 140^\circ$*, dip* $= 70^\circ$ *and rake* $= -10^\circ$*. The epicenters of the main shock (large asterisk), foreshocks (squares) and best-located aftershocks (circles) are also plotted. The main shock focal mechanism is shown as lower-hemisphere equal-area projection. The stress changes are shown by contours of 0.1 bar: with for receiver faults striking between* 120° *and* 160° *(b), dipping between* 50° *and* 90° *(c), and slip angles between* 0° *and* -30° *(d).* ΔCFF *for* μ *in the range of* $0.2 - 0.9$ *(e),* B *between 0.5 and 0.9 (f), calculation depths between 8 and 15 km (g), strikes of the fault plane between* 138° *and* 158° *(h), dips of the fault plane between* 50° *and* 90° *(i) and rakes of the fault plane between* -20° *and* 20° *(j) (source: [KAR 03]). For a color version of this figure, see www.iste.co.uk/votsi/multistate.zip*

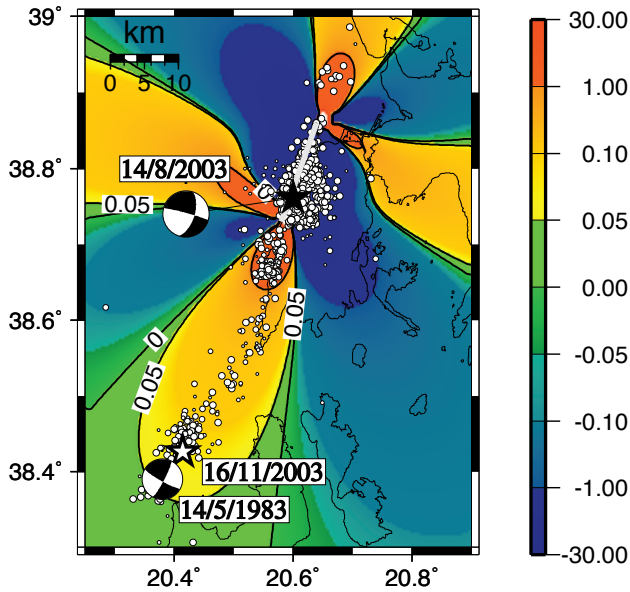

Figure 1.9. *Static stress changes (in bars) caused by the coseismic slip of the 2003 Lefkada main shock (solid star) are calculated at a depth of 8 km with* $\mu' = 0.6$ *for a typical fault plane solution for this place (strike* $= 28^o$*, dip* $= 82^o$ *and rake* $= 172^o$*). Contours denote values of 0, 0.05 and 1 bar. The white thick line represents the main rupture. Aftershocks (small circles) not related to the main rupture are mostly located in stress-enhanced areas. Two clusters of aftershocks, south and north of the main rupture, are inside areas with stress changes higher than 1 bar. The November 16, 2003 epicenter (open star) and the May 14, 1983 fault plane solution are also plotted (modified from [KAR 04]). For a color version of this figure, see www.iste.co.uk/votsi/multistate.zip*

The probability distribution of the proportion of aftershocks to occur in these areas independently of the stress changes was chosen by the use of a non-parametric kernel density estimator for their spatial distribution. Separate analyses were carried out for areas with positive values of stress change larger than or equal to 0.1, 0.3, 1.0, 5.0 and 10.0 bar and for those with negative values of stress

change smaller than or equal to –0.1, –0.3, –1.0, –5.0 and –10.0 bar. The tests have indicated, very confidently, a probability increase for aftershocks to be generated inside areas of increased stress, showing triggering caused by the static stress change. The analysis, however, has not provided arguments to approve the inclusion of stress shadows inside areas of larger values of negative stress change. A statistically significant increase of the probability was estimated for earthquakes inside stress changes less than or equal to –5.0 and –10.0 bar. In locations with larger absolute values of stress change, this probability increases regardless of the sign of the change. Nevertheless, this is more prevalent in areas of positive change than in those of negative change [LAS 09].

The location of some aftershocks in regions of negative static stress changes might be attributed to the facts that the slip model is much simpler than the real one and the details of the crustal heterogeneities are not taken into account, and due to the activation of several small faults with geometries different from the dominant one. When seeking stress shadows, a problem obscuring statistical analysis is associated with the fact that the background seismicity is usually quite sporadic and, consequently, the required statistically significant postseismic rate decrease cannot be obtained.

1.5.3. *Triggering of mining seismicity*

The evaluation of seismic hazard in mining areas comprises both societal and scientific components, given that the risk in the nearby built environment is high even from low- or moderate-magnitude earthquakes, and the earthquake occurrence is comparatively high. It has been

shown that the activity is time-dependent and that small stress changes are capable of encouraging or discouraging the anticipated seismicity. These interactions among mining-induced earthquakes in the Rudna Mine of the Legnica-Glogów Copper District in south-west Poland were investigated using Coulomb stress changes calculations [ORL 09]. These stress changes are not capable of inducing new tremors, since they are just a small percentage of the stress field in mining areas. Nevertheless, when the rock mass at the nucleation point is close to failure, it can then be further encouraged. For each investigated case, cumulative static stress changes caused by the previous earthquakes with energy greater than 105 J and with a known focal mechanism that occurred in the LGCD area during 1993–1999 were calculated.

These calculations were performed according to the focal mechanism of the target rupture, i.e. the next occurrence in the dataset. The stress was considered to be equal to zero before the occurrence of the first event, when the calculations were started. At each step of the calculation, the correlation between the derived stress field and the earthquake locations was sought. The results indicated that very often mining earthquakes may cause stress changes that are capable of triggering other shocks nearby. In this case, a large percentage of the shocks, reaching up to 60%, are inside areas with positive values of stress changes, with most of them being located in regions of positive ΔCFF above 0.01 MPa. Even in the cases where the earthquake foci are inside areas of negative Coulomb stress changes, most of the ruptured zones are partially inside stress-enhanced areas, which further shows the possible triggering at the nucleation location.

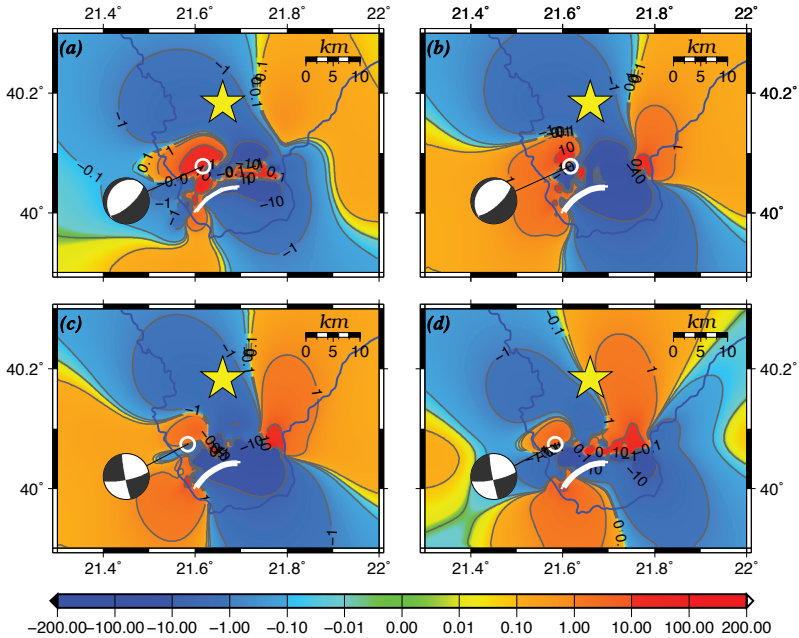

Figure 1.10. *Coulomb stress changes due to a detailed coseismic slip model [RES 05] for the Kozani-Grevena main shock, the epicenter of which is shown by the large star. The Coulomb stress changes, indicated by the gray scale and contours, were calculated (in bars) according to the characteristics of both nodal planes of each aftershock which are plotted as small white circles. The focal mechanisms are shown as lower-hemisphere equal-area projections. Calculations were performed for the (a) north-dipping and (b) south-dipping nodal planes of the normal faulting aftershock (210/21/-90, 50/70/-83) that occurred on 1995/05/20 at 04:46:31.18, with $M = 2.5$, normal faulting aftershock (210/21/-90, 50/70/-83) and 7.57 km depth. The stress changes are distributed in a different way, and in the first case, the event is encouraged (37.64 bar at its hypocenter), whereas in the second case, it is discouraged (-4.65 bar). Analogously, different distributions are derived for (c) the E-W-oriented and (d) the N-S-oriented nodal planes of the strike-slip aftershock (78/78/-5, 169/85/-168) that occurred on 1995/05/24 at 22:09:17.99, with $M = 2.8$ at 7.01 km depth. The earthquakes occurred in positive static stress changes for both cases, 1.0 and 3.97 bar, respectively (source: [LAS 09]). For a color version of this figure, see www.iste.co.uk/votsi/multistate.zip*

1.6. Discussion on stress interaction

Interaction between faults is studied by calculating the changes in their associated stress field. The first achievements in the Landers earthquake sequence prove that Coulomb stress calculations might constitute a powerful tool for assessing the interaction between strong events and main shocks with their aftershocks. Convincing evidence is furthermore found between Coulomb stress changes and seismicity rate variations for several years after the occurrence of strong earthquakes. It appears that Coulomb stresses even equal to 0.1 bar are capable of influencing the aftershock locations (see [HAR 00] and the references therein). This value is a small percentage of the stress drop during an earthquake occurrence, which explains why the expressions "enhancement" and "encouragement" are more appropriate than earthquake generation. The effectiveness of the stress changes being much smaller than the stress drops during a failure, to influence the seismicity behavior and to enhance or discourage the occurrence of moderate to large subsequent events, is correlated with the state of stress on the target faults and whether these changes in stress are capable of advancing or delaying the next failures [GOM 00]. The earthquake triggering is not a function of the static stress changes alone, but also of other factors similar to the current stage of the seismic cycle on the target fault. In the case that a fault is at an early stage of its seismic cycle, the Coulomb stress changes are not efficient in triggering the next rupture.

Modeling of Coulomb stress changes assumes that a fault is locked during the interseismic period and is continuously loading and the change in the time for the next rupture (either advance or delay, Δt) that is caused by the static stress step is not influenced by the time it happens. This means that the earthquakes triggered by a clock advance would have taken place later in time. One question of paramount importance is whether a static stress change

threshold exists, above which triggering takes place. Then, which among the areas where such changes were calculated are more prominent for earthquake nucleation? How imminent will the triggered earthquake be and why are there "delayed" triggered earthquakes? Is it feasible and in which way is stress enhancement adequate to trigger earthquakes on otherwise inactive faults? Static stress change that is smaller than 0.1 bar and that is adequate to influence subsequent earthquakes, by accelerating or delaying their occurrence, is continuously under investigation. Several cases exist where smaller values of stress changes are obviously correlated with seismicity distribution. Another important contribution to the long-term loading process arises from the viscoelastic relaxation of the lithosphere and asthenosphere, which is caused by coseismic stress perturbations and influences the long-term time-dependent stress transfer. It may enhance the amplitude and the extent of negative stress changes on a short time scale because of the relaxation process taking place below the seismogenic layer, and it would also reload the entire crust over longer time scales. In general, it is worth noting here that viscoelastic relaxation processes, poroelastic effects (fluid flow, for instance), creep and rate- and state-dependent friction influence the postseismic stress distribution in ways that cannot yet be fully explained.

Theoretical models have been developed to answer the aforementioned and related questions. Nevertheless, the mechanisms involved in the nucleation of triggered earthquakes are complex, and the impact of the changes in the stress field caused by the slip during the strong earthquake occurrence, with the influence of the stress changes associated with coseismic slip along with the long-term slip rates on all known causative seismogenic faults, where strong earthquakes might be anticipated, is difficult to be unequivocally calculated. It then becomes necessary to approach the fault interaction through proper

tools of statistical analysis with which the hidden stress state will be revealed. The combination of appropriate catalog of earthquakes, associated with specific fault populations with distinctive seismotectonic properties in selected areas, and modeling stress interactions in these fault populations along with proper statistical tools, has yielded promising results in revealing earthquake generation patterns [VOT 13, PER 16].